JCTC Journal of Chemical Theory and Computation

Article

pubs.acs.org/JCTC

Deconstructing the ONIOM Hessian: Investigating Method Combinations for Transition Structures

Thom Vreven,[†,‡] Lee M. Thompson,[§] Susan M. Larkin,[§] Ian Kirker,[∥] and Michael J. Bearpark*[,§]

[†]Gaussian, Inc., 340 Quinnipiac St Bldg 40, Wallingford, Connecticut 06492, United States

[‡]Program in Bioinformatics and Integrative Biology, University of Massachusetts Medical School, Worcester, Massachusetts 01605, United States

[§]Department of Chemistry, Imperial College, London, SW7 2AZ, United Kingdom

[∥]Department of Chemistry, University College, London, WC1H 0AJ, United Kingdom

Supporting Information

ABSTRACT: Developments in biochemistry and materials sciences have led to increasing interest in the reactivity of large chemical systems, presenting theoretical and computational challenges that can be addressed with hybrid methods such as ONIOM. Here, we show that the diagonalized ONIOM Hessian can be partitioned/deconstructed into contributions from the individual subcalculations—indicating the curvature of their potential energy surfaces (PESs)—without increasing the computational cost. The resulting pseudofrequencies have particular application in the study of transition structures and higher-order saddle points with ONIOM, where we find that an imaginary frequency may result from combining subcalculations for which the corresponding vibrational frequencies are all real. Two cycloaddition reactions, including functionalization of a 150 atom (5,5) single-walled carbon nanotube, demonstrate how this analysis of pseudofrequencies allows identification of critical points where further exploratory work should be carried out to ensure that the ONIOM PES correctly approximates the target.

INTRODUCTION

Chemical reactivity can be studied computationally by locating critical points on potential energy surfaces (PESs). The minima represent equilibrium structures and intermediates, which are connected by the transition structures (TSs) that are defined as first order saddle points on the PES. The reaction pathways are then determined by the relative energies of the reactants, intermediates, and products, and the activation energies that are needed to transition between them.[1,2]

Computationally expensive quantum mechanical (QM) methods are needed for the accurate calculation of the geometries and energies of the critical points. This is particularly the case for TSs that involve bond breaking and formation, for which treatment of electron correlation is generally more important than for equilibrium structures. Also, for the geometry optimization algorithms and characterization of the resulting critical points, we need an accurate representation of the curvature (from second derivatives) of a potential energy surface, which again is more critical for transition structure searches than for the search for equilibrium structures. However, the computational resources needed for the calculation of the Hessian elements increases quickly and nonlinearly with the size of the system. Reactivity studies of systems encountered in biochemistry and materials therefore become prohibitively expensive with any conventional QM method.

There are two traditional approaches to reduce the computational times needed for such large chemical systems. First, one can use a more approximate (lower) level of theory to treat the entire system. Second, when the process being investigated takes place in a distinct, localized part of the system, high-level calculations can be performed on a truncated model. Each of these two approximations has its obvious limitations; the former does not treat the reactive center at a sufficiently high level of theory, while the latter excludes electronic and steric effects from the part of the molecule that is not included in the truncated model (i.e., the substituent effect).

During the past decade, a third approach has become popular for the study of large molecular systems, which combines both traditional approaches described. In this hybrid approach, the full system is divided into a reactive part, which is treated at an appropriately high level of theory computationally, while the remainder of the system is included at a less expensive lower level of theory. This ensures an appropriately high level of accuracy for the reactive part of the system, while reducing the computational cost by only calculating this smaller part with the expensive method.

The best-known class of hybrid methods is formed by the quantum mechanics/molecular mechanics (QM/MM) schemes,[3−6] which combine a quantum mechanical (QM) method with a molecular mechanics (MM) method. QM/MM methods have primarily been used to study processes that require a QM treatment in which the environment plays an important steric or electrostatic role and yet is too large to include at this level: for example, reaction pathways, explicit solvent effects, and excited states.[7−9]

Special Issue: Berny Schlegel Festschrift

Received: July 18, 2012
Published: October 2, 2012

An alternative hybrid method is ONIOM, which is a generalized scheme for layered calculations.[10−16] Whereas QM/MM calculations combine a QM method with an MM method, ONIOM can combine QM methods with other QM methods, as well as QM and MM methods. Furthermore, ONIOM can, in principle, combine any number of methods, although the current implementation is limited to three.[17−19] The ONIOM potential is well-defined for both the energy and its derivatives, and hence permits optimization of both minima and TSs, as well as the calculation of normal modes and vibrational frequencies.[20,21] Several studies have shown the utility of ONIOM in locating and characterizing TSs in agreement with the target (defined as the high-level calculation on the full system) while reducing computational cost.[22,23]

In this work, we analyze the curvature of the ONIOM potential surface at transition structures, by deconstructing the ONIOM Hessian after it has been assembled and diagonalized, generating vibrational pseudofrequencies for the individual subcalculations. To test our approach, we present two case studies involving Diels−Alder cycloaddition reactions. First, we examine the cycloaddition of quinodimethane to a (5,5) single-walled nanotube (SWNT). This system has been studied previously using the ONIOM method by Lu et al.;[24] however, by analyzing the pseudofrequencies of the vibrational modes with imaginary frequencies, we are able to understand the role of the ONIOM partition and method combination in determining the shape of the PES. Second, we consider the prototype cycloaddition of cyclohexadiene and maleic anhydride. Here, we found that a particular method combination in ONIOM results in a second order saddle point, where both the target and calculations with either a truncated model system or a reduced level of theory on the full system indicated a first order saddle point. This unexpected disagreement was the initial motivation for the current work. For both case studies, we compare ONIOM results to the target: a full conventional calculation.

COMPUTATIONAL METHODS

A. ONIOM Method. The ONIOM energy is written as an extrapolation:

$$E^{ONIOM} = E^{high}_{model} + E^{low}_{real} - E^{low}_{model} \tag{1}$$

high and low refer to the levels of theory that are combined in ONIOM; real refers to the full system, and model to the part of the system that is treated at the high level of theory. The model system is calculated at both levels of theory, while the real system is calculated only at the low level of theory. All three terms in expression 1 involve chemically realistic systems, which allows the low level to be either QM or MM, thus forming ONIOM(QM:QM′) as used in this work, or ONIOM(QM:MM).

Dangling bonds resulting from covalent bonding between the model and its surroundings are saturated with link atoms. The centers that exist in both the model and real systems have the same coordinates, and the positions of the link atoms are a function of the geometry of the full system. The gradients and higher derivatives are therefore well-defined, and can be obtained with expressions similar to that for the energy:

$$\frac{\partial E^{ONIOM}}{\partial \mathbf{q}} = \frac{\partial E^{high}_{model}}{\partial \mathbf{q}_m}\mathbf{J} + \frac{\partial E^{low}_{real}}{\partial \mathbf{q}} - \frac{\partial E^{low}_{model}}{\partial \mathbf{q}_m}\mathbf{J} \tag{2a}$$

$$\mathbf{H}^{ONIOM} = \frac{\partial^2 E^{ONIOM}}{\partial \mathbf{q}^2} = \mathbf{J}^T\frac{\partial^2 E^{high}_{model}}{\partial \mathbf{q}^2_m}\mathbf{J} + \frac{\partial^2 E^{low}_{real}}{\partial \mathbf{q}^2} - \mathbf{J}^T\frac{\partial^2 E^{low}_{model}}{\partial \mathbf{q}^2_m}\mathbf{J} \tag{2b}$$

$\mathbf{J}$ is the Jacobian matrix that projects the forces of the model system (link) atoms onto the coordinate space of the full system. For geometry optimization or other ways to explore the potential surface we use the integrated energy and derivatives from expressions 1 and 2.

B. Deconstructing the ONIOM Hessian. In the study of transition structures, crucial quantities are the transition vector and the curvature of the potential energy surface along it. The transition vector is obtained by mass-weighting and diagonalizing the Hessian $\mathbf{H}$. In an ONIOM calculation, we mass-weight and diagonalize the ONIOM Hessian $\mathbf{H}^{ONIOM}$ (from expression 2b). This is assembled from subcalculations that may not be located at stationary points on their own potential energy surfaces, but the transformation is nevertheless valid because the overall ONIOM gradient is zero. The curvature of the surface along a normal mode is related to the corresponding eigenvalue. In the remainder of this section we will show how we can write the ONIOM transition vector (and other vibrational modes) in such a way that the individual contributions can be analyzed.

A normal mode $\mathbf{X}_i$ is defined as an eigenvector of the (mass-weighted) Hessian $\mathbf{H}$.

$$\mathbf{H}\mathbf{X}_i = \alpha_i\mathbf{X}_i \tag{3}$$

$\mathbf{H}$ is an $N \times N$ matrix, where N is the number of Cartesian variables. $\mathbf{X}_i$ is a vector with N elements. α_i is the eigenvalue for the mode $\mathbf{X}_i$, and is a measure of the curvature of the mass-weighted potential surface in the direction of this mode. We can collect all the normal modes $\mathbf{X}_i$ into a matrix, $\mathbf{X}$:

$$\mathbf{H}\mathbf{X} = \mathbf{X}\boldsymbol{\alpha} \tag{4}$$

Now $\mathbf{X}$ is an $N \times N$ matrix (with columns $\mathbf{X}_i$), and $\boldsymbol{\alpha}$ is a diagonal $N \times N$ matrix containing the eigenvalues α_i. Since we use a mass-weighted Hessian, the vectors $\mathbf{X}_i$ are the vibrational modes. The frequency corresponding to a vibrational mode is defined as

$$f_i = \sqrt{\alpha_i} \tag{5}$$

When the system is at a minimum, the eigenvalues α_i are all positive. Here, we do not include the 5 or 6 translational and rotational modes that have zero eigenvalues. At a transition structure, one eigenvalue is negative (corresponding to an imaginary frequency), while the remaining eigenvalues are positive. The transition vector is the vibrational mode associated with the negative eigenvalue.

Because the potential energy surface is well-defined in the ONIOM scheme, the second derivative matrix (Hessian) can be calculated. This Hessian can then be used to obtain the vibrational modes. As for the energy and gradient, the ONIOM Hessian is written in terms of the Hessians from the three subcalculations

$$\mathbf{H}^{ONIOM} = \mathbf{H}^{high}_{model} + \mathbf{H}^{low}_{real} - \mathbf{H}^{low}_{model} \tag{6}$$

Since the coordinates of the model system are derived from those of the full system, the ONIOM Hessian matrix $\mathbf{H}^{ONIOM}$ is of dimension $N \times N$. The Hessian matrices from the model system, $\mathbf{H}^{high}_{model}$ and $\mathbf{H}^{low}_{model}$, are sparse, since only elements that

involve atoms from the model region will be nonzero. In expression 6, the individual terms are assumed to be mass-weighted, and the elements corresponding to link atoms projected onto the real atoms, as for expression 2.[16]

Just as in expression 4, we can diagonalize the ONIOM Hessian matrix, $\mathbf{H}^{\mathrm{ONIOM}}$:

$$\mathbf{H}^{\mathrm{ONIOM}}\mathbf{X}^{\mathrm{ONIOM}} = \mathbf{X}^{\mathrm{ONIOM}}\boldsymbol{\alpha}^{\mathrm{ONIOM}} \tag{7}$$

$\mathbf{X}^{\mathrm{ONIOM}}$ and $\boldsymbol{\alpha}^{\mathrm{ONIOM}}$ are the eigenvectors and eigenvalues, respectively. The number of resulting eigenvectors and eigenvalues is identical to that from diagonalization of the conventional Hessian in expression 4.

To deconstruct the ONIOM Hessian, we use expression 6 to write $\mathbf{H}^{\mathrm{ONIOM}}$ in terms of the individual contributions, and multiply both sides with the transpose of matrix $\mathbf{X}^{\mathrm{ONIOM}}$ containing the eigenvectors ($\mathbf{X}^{\mathrm{ONIOM}}$ is a transformation matrix, and $\mathbf{X}^{t,\mathrm{ONIOM}}\mathbf{X}^{\mathrm{ONIOM}} = \mathbf{I}$):

$$\begin{aligned}&\mathbf{X}^{t,\mathrm{ONIOM}}\mathbf{H}^{\mathrm{high}}_{\mathrm{model}}\mathbf{X}^{\mathrm{ONIOM}} + \mathbf{X}^{t,\mathrm{ONIOM}}\mathbf{H}^{\mathrm{low}}_{\mathrm{real}}\mathbf{X}^{\mathrm{ONIOM}}\\ &\quad - \mathbf{X}^{t,\mathrm{ONIOM}}\mathbf{H}^{\mathrm{low}}_{\mathrm{model}}\mathbf{X}^{\mathrm{ONIOM}}\\ &\quad = \boldsymbol{\alpha}^{\mathrm{ONIOM}}\end{aligned} \tag{8}$$

We define the following matrices:

$$\boldsymbol{\beta}^{\mathrm{high}}_{\mathrm{model}} = \mathbf{X}^{t,\mathrm{ONIOM}}\mathbf{H}^{\mathrm{high}}_{\mathrm{model}}\mathbf{X}^{\mathrm{ONIOM}} \tag{9}$$

$$\boldsymbol{\beta}^{\mathrm{low}}_{\mathrm{real}} = \mathbf{X}^{t,\mathrm{ONIOM}}\mathbf{H}^{\mathrm{low}}_{\mathrm{real}}\mathbf{X}^{\mathrm{ONIOM}} \tag{10}$$

$$\boldsymbol{\beta}^{\mathrm{low}}_{\mathrm{model}} = \mathbf{X}^{t,\mathrm{ONIOM}}\mathbf{H}^{\mathrm{low}}_{\mathrm{model}}\mathbf{X}^{\mathrm{ONIOM}} \tag{11}$$

Thus:

$$\boldsymbol{\alpha}^{\mathrm{ONIOM}} = \boldsymbol{\beta}^{\mathrm{high}}_{\mathrm{model}} + \boldsymbol{\beta}^{\mathrm{low}}_{\mathrm{real}} - \boldsymbol{\beta}^{\mathrm{low}}_{\mathrm{model}} \tag{12}$$

Although $\boldsymbol{\alpha}^{\mathrm{ONIOM}}$ is diagonal, the matrices $\boldsymbol{\beta}$ are not, because $\mathbf{X}^{\mathrm{ONIOM}}$ contains the eigenvectors obtained with $\mathbf{H}^{\mathrm{ONIOM}}$, and not the individual components of the ONIOM Hessian. We can, however, split each matrix $\boldsymbol{\beta}$ into a diagonal matrix $\boldsymbol{\gamma}$ and an off-diagonal matrix $\boldsymbol{\omega}$:

$$\begin{aligned}\boldsymbol{\alpha}^{\mathrm{ONIOM}} &= (\boldsymbol{\gamma}^{\mathrm{high}}_{\mathrm{model}} + \boldsymbol{\omega}^{\mathrm{high}}_{\mathrm{model}}) + (\boldsymbol{\gamma}^{\mathrm{low}}_{\mathrm{real}} + \boldsymbol{\omega}^{\mathrm{low}}_{\mathrm{real}})\\ &\quad - (\boldsymbol{\gamma}^{\mathrm{low}}_{\mathrm{model}} + \boldsymbol{\omega}^{\mathrm{low}}_{\mathrm{model}})\end{aligned} \tag{13}$$

Because $\boldsymbol{\alpha}^{\mathrm{ONIOM}}$ is diagonal, the sum of the off-diagonal matrices $\boldsymbol{\omega}$ must be zero, thus:

$$\boldsymbol{\alpha}^{\mathrm{ONIOM}} = \boldsymbol{\gamma}^{\mathrm{high}}_{\mathrm{model}} + \boldsymbol{\gamma}^{\mathrm{low}}_{\mathrm{real}} - \boldsymbol{\gamma}^{\mathrm{low}}_{\mathrm{model}} \tag{14}$$

The (diagonal) elements γ_i of (diagonal) matrices $\boldsymbol{\gamma}$ are again measures of the curvature in the direction of each normal mode, but are now separate for each of the ONIOM contributions. Expression 14 simply means that the ONIOM curvature along a vector can be obtained from the three individual curvatures, similar to other quantities such as the energy. However, these curvatures are along normal modes that are obtained with the full ONIOM Hessian, and not from diagonalizing the individual Hessian matrices. Therefore we cannot call elements γ_i eigenvalues.

Just as the frequency f_i is related to the eigenvalue α_i, we can also take the square root of γ_i, for example:

$$f'^{\mathrm{low}}_{\mathrm{model},i} = \sqrt{\gamma^{\mathrm{low}}_{\mathrm{model},i}} \tag{15}$$

We use the tick-mark in f' to indicate that it is a pseudofrequency. Equivalently to the energy (expression 1), gradient (expression 2a), and Hessian (expressions 2b and 6), we can now express the ONIOM frequency as a combination of three components:

$$f^{\mathrm{ONIOM}}_i = (f'^{\mathrm{high}}_{\mathrm{model},i})^2 + (f'^{\mathrm{low}}_{\mathrm{real},i})^2 - (f'^{\mathrm{low}}_{\mathrm{model},i})^2 \tag{16}$$

Note that f^{ONIOM}_i is the actual ONIOM frequency, for a normal mode obtained from the ONIOM Hessian, and therefore does not have a tick-mark. We can now analyze ONIOM frequency values in the same way as we usually examine ONIOM energetics, and observe the effect of the substituents on the frequency. As we will show in the Results and Discussion section of this article, this is of particular value when investigating the behavior of ONIOM for transition structures.

The analysis presented in its current form has been tested for ONIOM(QM:QM′). Other multiscale methods often use Molecular Mechanics methods in the low level, for which bond-breaking and bond-forming potentials are in general not defined. In addition, multiscale methods besides ONIOM that can have QM methods in the low level often have a more complicated energy function than eq 1, which requires modification of our approach.

C. Case Studies. To demonstrate our method for the analysis of ONIOM frequencies, we investigated two Diels–Alder cycloadditions as test systems: quinodimethane with a (5,5) SWNT, and maleic anhydride with cyclohexadiene.

A complication of ONIOM applied to nanotubes is the extended aromatic system. In general it is not recommended[25] to cut through aromatic systems in the partition of a system into high- and low-level layers, but in this case it cannot be avoided. Osuna et al.[26] studied a number of partitions in the Diels–Alder reaction between cyclopentadiene and C_{60} fullerene and found that a model including four rings from the extended surface was acceptable in terms of cost and reproducing target energies and geometries.

Critical points were characterized using analytical frequency calculations, including the pseudofrequency deconstruction described in the section above. Intrinsic Reaction Coordinates (IRCs) were used to link TSs to the reactants and products, and were carried out using the Hessian-based Predictor-Corrector integrator algorithm.[27,28] We used a modified version of the development version of Gaussian for quantum mechanical calculations.[18]

RESULTS AND DISCUSSION

A. Diels–Alder Cycloaddition of Quinodimethane to a (5,5) SWNT. Developments in material sciences have yielded new materials based on extended unsaturated carbon systems, such as graphenes, fullerenes, and nanotubes. These systems possess unique structural and electronic properties[29,30] although the relative inertness and low solubility of these structures has partially inhibited their use in practical applications to date. For this reason, the development of methods for the functionalization of nanotube sidewalls are desirable.[31−33]

Theoretical simulation may be used to determine the potential of a given synthetic route by determining the size of the activation barrier, which requires the calculation of transition structures. The properties of these systems arise from the extended delocalized electronic structure, and QM methods are required for their description. However, a full quantum treatment at a sufficiently high level of theory is extremely time-consuming due to the size of the system. The

dx.doi.org/10.1021/ct300612m | J. Chem. Theory Comput. 2012, 8, 4907−4914

ONIOM(QM:QM′) method is, therefore, particularly suited to the study of these systems, as it allows the substituent effect to be included at a semiempirical or quantum level, reducing the computational cost while capturing the electronic effect.

A survey of the literature reveals that ONIOM is indeed widely used to locate and characterize TSs for addition reactions of carbon nanostructures. A number of reactions involving fullerenes have been studied using ONIOM(B3LYP/6-31G(d):SVWN/STO-3G), including retro-cycloadditions of substituted fullerenes,[34,35] addition of thiols and alcohols,[36,37] and [4 + 2] cycloadditions.[26,38,39] Lu et al. have used AM1 as the low level in conjunction with B3LYP/6-31G(d) to study the viability of various dieneophiles in cycloadditions to nanotubes.[24,40,41] This combination has also been used to study the addition of aryl diazonium salts to SWNTs and adsorption of CO and O onto graphene.[42,43] PM3 has also been used to model the substituent effect in calculating barriers of carbene, silylene, germylene, and diazomethane addition to nanotubes,[44,45] while other studies have used UFF in the study of aliphatic amine additions to functionalized nanotube tips[46−48] and NO addition at defects in SWNTs.[49] Apart from direct functionalization of the carbon structure, ONIOM has been used to study the role of nanotube encapsulation of reagents in changing barrier heights and controlling reaction kinetics.[50−52] 1,3-cycloadditions to graphene could also be studied using ONIOM[53,54] as an alternative to density functional theory alone.[55]

Our tests on the SWNT cycloaddition are based on the work by Lu et al.,[24] who studied the reaction energies of cycloaddition between a $C_{130}H_{20}$ (5,5) SWNT and the reactive dienophile quinodimethane. The high-level layer in Lu's work consisted of the quinodimethane and four fused rings of the SWNT (referred to as QM42 in our work, as the model system contains 42 atoms) and was treated at the B3LYP/6-31G(d) level of theory, while the remainder of the system was treated at the AM1 level of theory (Figure 1A). In addition to Lu's partition, we also considered a reduced high-level layer (referred to as QM16, Figure 1B).

Lu presented a symmetric transition structure with the QM42 partition, suggesting that the reaction takes place via a concerted pathway. We have re-examined this transition structure and carried out further analysis by calculating the ONIOM frequencies in terms of the contributions of the individual subcalculations. We found that, for the QM42 partition, the symmetric/synchronous transition structure actually corresponds to a second-order saddle point (Figure 1A, C), while a slightly lower in energy (Table 1) first-order transition structure was found to be antisymmetric/asynchronous (Figure 1D). The two saddle points are closely related to each other: we found a barrierless energy profile along the linear interpolation between the two structures.

For the symmetric saddle point, we show in Table 2 the frequencies of the lowest two modes calculated using the various levels of theory and ONIOM partitions. In all calculations, these two modes corresponded to a symmetry conserving mode, leading to concerted bond formation, and a symmetry-breaking mode. We also show the contributions of the subcalculations for the ONIOM calculations. Surprisingly, we find that each of the three ONIOM subcalculations give positive pseudofrequencies for the symmetry-breaking mode 2. Only when they are combined, according to expression 16, does the curvature become negative. When we used the low level of theory (AM1) on the full system separately, we found a

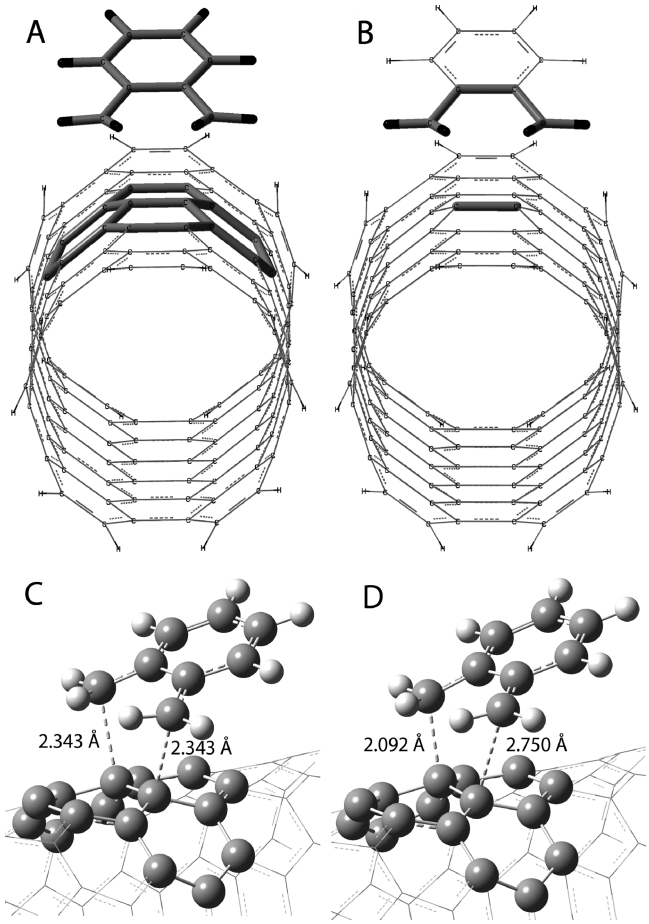

Figure 1. ONIOM partitions for the cycloaddition of quinodimethane to a 150-atom (5,5) SWNT calculated using the QM42 model system (A) and the smaller model system QM16 (B), with the high level layer rendered graphically by tubes. Close-ups of the QM42 model system show the difference between the symmetric (C) and asymmetric (D) transition states.

Table 1. Relative Energies (kcal.mol^{-1}) for the (5,5) SWNT and Quinodimethane Diels-Alder Reaction, Determined with ONIOM(B3LYP/6-31G(d):AM1) Using the QM42 Partition (Figure 1A)[a]

structure	ONIOM	model(AM1)	model(B3LYP)	real(AM1)
reactants	0.00	0.00	0.00	0.00
symmetric TS	19.20	33.39	24.67	27.92
asymmetric TS	18.99	35.57	23.91	30.65
product	−28.76	−4.81	−9.99	−23.57

[a]In addition to the ONIOM energies, we also show the energies of its components.

first order saddle point, which is qualitatively in agreement with the AM1 ONIOM subcalculation on the real system.

Based on the fact that the ONIOM pseudofrequencies for the second mode are all real, one could argue that the observed imaginary frequency may be 'spurious'. To test this, we carried out the optimization and vibrational analysis on the target (the high-level calculation on the entire system) to determine whether ONIOM represents the target correctly, or whether the second imaginary frequency is incorrectly introduced by the combination of different methods. The target calculation showed that, in agreement with ONIOM, the symmetric TS

dx.doi.org/10.1021/ct300612m | J. Chem. Theory Comput. 2012, 8, 4907−4914

Table 2. Frequency Analysis of the Symmetric Transition Structure in the (5,5) SWNT and Quinodimethane Diels–Alder Reaction, Determined Using AM1, B3LYP/6-31G(d), and ONIOM(B3LYP/6-31G(d):AM1) Using Partitions QM42 (Figure 1A) and QM16 (Figure 1B)

	mode 1	mode 2
$f^{low}_{real,i}$	783i	38
$f^{high}_{real,i}$ (target)	461i	101i
$f_i^{ONIOM,QM42}$	552i	29i[a]
$f'^{low,QM42}_{model,i}$	281	230
$f'^{high,QM42}_{model,i}$	313i	88
$f'^{low,QM42}_{real,i}$	358i	210
$f_i^{ONIOM,QM16}$	334i	27
$f'^{low,QM16}_{model,i}$	666i	129
$f'^{high,QM16}_{model,i}$	489i	52
$f'^{low,QM16}_{real,i}$	563i	121

[a]Due to rounding errors that become large as we take the differences of squares, this value is not consistent with the rounded values of the pseudofrequencies listed in this table. In the Supporting Information, we show the values with higher precision, which are consistent according to eq 16.

is a second order saddle point with frequencies of 461i cm^{-1} and 101i cm^{-1}. Thus, the ONIOM QM42 calculation produces the correct second order saddle point, despite all the individual frequency components of the second mode having positive curvature. In Table 1 we also list the individual contributions to the ONIOM energies. Both low level (AM1) contributions raise the energy of the asymmetric TS relative to the symmetric TS, which agrees with the sign of the pseudofrequencies (both are real). However, the energy of the real system contribution rises more (2.7 kcal·mol^{-1}) than the model system (2.2 kcal·mol^{-1}), which is in contrast with the magnitude of the low level pseudofrequencies (larger for the model system than for the real system). Furthermore, the high level contribution to the symmetric TS is lower than for the asymmetric TS, which is in contrast with the real pseudofrequency of the high level contribution. Although the ONIOM frequency agrees with a lower lying asymmetric TS, it is clear that anharmonic contributions play a role in the actual energy difference between the symmetric TS and asymmetric TS.

In addition, we tested a smaller model system (QM16, Figure 1B) to assess whether a change in the ONIOM partition, and not the method combination, can change the nature of the symmetric saddle point. The two lowest frequency normal modes were found to be 334i and 27 cm^{-1}, indicating that the choice of partition can qualitatively affect the ONIOM potential energy surface (by changing the curvature of the asymmetric mode 2 in this case).

The goal of ONIOM is the reduction of computational cost in terms of wall time and memory requirements. On our machines, a single ONIOM energy with gradient evaluation on the (5,5) SWNT + quinodimethane system requires about 1% of the computational time required for the target calculation. The high-level calculation on the model system represents the bottleneck here, taking about 90% of the computational time. The corresponding frequency calculation using the ONIOM scheme requires about 1% of the target computational time, but here the memory requirements are reduced by 2 orders of magnitude (from 360GB to several GB). Thus, depending on the type of calculation, ONIOM can significantly reduce both computational time and memory space requirements.

B. Diels–Alder Cycloaddition of Cyclohexadiene and Maleic Anhydride. We carried out exploratory calculations using ONIOM for the addition of cyclohexadiene and maleic anhydride, with a model system that consists of the butadiene + ethene fragment where the bond breaking and formation takes place. Our target level of theory was CASSCF in this case,[56] and we used the ONIOM method with CASSCF (6 electrons in six π orbitals) for the model system and HF for the remainder of the system.

Surprisingly, using ONIOM(CASSCF/STO-3G:HF/STO-3G), the TS search under C_s symmetry yields a second order saddle point (Figure 2, Table 3), while we obtain first order

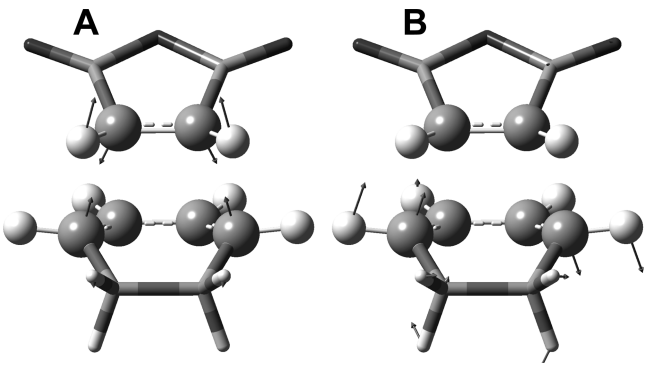

Figure 2. C_s Diels–Alder transition structure for cyclohexadiene and maleic anhydride at the ONIOM(CASSCF/STO-3G:HF/STO-3G) level of theory. The CASSCF layer is represented by ball-and-stick, and the HF layer by tube. The displacement vectors in panel A correspond to the symmetric stretch at 936i cm^{-1}, and in panel B to the asymmetric bend at 65i cm^{-1}.

saddle points when we optimize for the TS using either conventional CASSCF/STO-3G or conventional HF/STO-3G, for either the full system or for the model system alone. Furthermore, changing the high-level method in the ONIOM calculation to CASSCF/4-31G also results in a first order saddle point (Table 3). In other words, the symmetric ONIOM(CASSCF/STO-3G:HF/STO-3G) stationary point is a second order saddle point with negative curvature along the symmetry distortion mode that is not present in any of the conventional calculations on the full or reduced system, and which appears very sensitive to the level of theory used in ONIOM.

Before analyzing the frequencies as outlined in the Computational Methods section, we first discuss the energetics of the reaction at the various levels of theory. Besides the frequencies, we show in Table 3 the activation energies and reaction energies, for both the full system and the truncated model system. We see that the HF and CASSCF barriers ΔE^{TS} are quite close with the same basis set (largest difference is 4 kcal·mol^{-1}). Also, we see that the reaction energy is much smaller (by several tens of kcal·mol^{-1}) with the 4-31G basis set than with the STO-3G basis set. The difference between the full system and the model system varies but is about 5 kcal·mol^{-1} for both the TS and reaction energy at the highest level of theory.

Comparing ONIOM to the target calculations (Table 4), we see that ONIOM(CASSCF/STO-3G:HF/STO-3G) is close to CASSCF/STO-3G, and ONIOM(CASSCF/4-31G:HF/4-31G) is close to CASSCF/4-31G, for both the barrier and reaction energy. In contrast, ONIOM(CASSCF/4-31G:HF/

Table 3. Cyclohexadiene and Maleic Anhydride Barrier and Reaction Energies (kcal·mol^{-1}) and Imaginary Frequencies (cm^{-1}) at the Various Levels of Theory, for Both the Full System (ONIOM and Conventional Methods) and the Model System (Butadiene and Ethene, Only Conventional Methods)

method	ΔE^{TS}	ΔE^{Reac}	imaginary frequencies	
CASSCF/STO-3G:HF/STO-3G (sym)	36.0	−53.1	936*i*	65*i*
CASSCF/STO-3G:HF/STO-3G (asym)	32.1	−53.1	1106*i*	
CASSCF/4-31G:HF/STO-3G	42.5	−2.4	733*i*	
CASSCF/4-31G:HF/4-31G	32.9	−14.6	728*i*	
HF/STO-3G	36.1	−87.3	855*i*	
HF/4-31G	31.3	−33.4	694*i*	
CASSCF/STO-3G	37.5	−56.7	960*i*	
CASSCF/4-31G	35.6	−16.5	764*i*	
HF/STO-3G (model only)	34.2	−106.5	968*i*	
HF/4-31G (model only)	39.6	−40.2	855*i*	
CASSCF/STO-3G (model only)	35.1	−72.4	1057*i*	
CASSCF/4-31G (model only)	41.1	−21.4	887*i*	

Table 4. Errors (kcal·mol^{-1}) Relative to the Target Levels of Theory, Using Various Systematic Approximations (Truncated and Method Refer to Truncating the Size of the System and Lowering the Level of Theory, Respectively)[a]

level of theory		ΔE^{TS} errors			ΔE^{Reac} errors		
target/high level	low level	ONIOM	truncated	method	ONIOM	truncated	method
CASSCF/STO-3G	HF/STO-3G	−1.6	−2.4	−1.4	3.6	−15.7	−30.6
CASSCF/4-31G	HF/STO-3G	7.0	5.5	0.5	14.1	−4.9	−70.7
CASSCF/4-31G	HF/4-31G	−2.6	5.5	−4.2	1.9	−4.9	−16.9

[a]Derived from Table 3.

STO-3G) is less close to the CASSCF/4-31G target calculation. The basis set used in the low-level region must, therefore, match that of the high-level in order for ONIOM to reproduce the target system energies.

We can also compare ONIOM with the calculation on the full system at the lower level of theory, or with the truncated system (the model) at the higher level of theory (Table 4). The errors are always larger than for ONIOM with the basis sets matched, except for the barrier calculated with ONIOM-(CASSCF/STO-3G:HF/STO-3G) compared to HF/STO-3G on the full system. However, in that case, both the ONIOM error and the error from using the low level of theory on the full system are very small (−1.6 and −1.4 kcal·mol^{-1}, respectively).

To conclude, ONIOM reproduces the target energies better than either the conventional alternatives of truncating the system or lowering the level of theory. ONIOM is well-behaved for this reaction, and the energetics do not show a problem that presages the extra imaginary frequency we observed. Clearly, correct energies in the symmetric space do not ensure the correct representation of the potential surface along symmetry breaking modes.

We analyzed the origin of the second imaginary frequency at the ONIOM(CASSCF/STO-3G:HF/STO-3G) level of theory using the pseudofrequencies. In Table 5, we show the integrated frequency for the first two normal modes (f_i^{ONIOM}) and the components from the three ONIOM subcalculations ($f'^{low}_{model,i}$, $f'^{high}_{model,i}$, and $f'^{low}_{real,i}$), with either the STO-3G basis set or the 4-31G basis set for CASSCF. All the contributions from the subcalculations to the second mode are real. However, the high level contributions from the model system are quite small (75−96 cm^{-1}), and the low level contributions can easily cause the sign to change. According to expression 16, the integrated frequency is related to the squares of the contributions from the subcalculations. For the calculation with the STO-3G basis set

Table 5. Frequencies of the Symmetric TS of cyclohexadiene and Maleic Anhydride Calculated with ONIOM and the Contributions from the Subcalculations (cm^{-1})

	CASSCF/STO-3G: HF/STO-3G	CASSCF/4-31G: HF/STO-3G		CASSCF/4-31G: HF/4-31G	
	mode 1	mode 1	mode 2	mode 1	mode 2
f_i^{ONIOM}	936*i*	65*i*[a]	733*i*	31	728*i*	42[a]
$f'^{low}_{model,i}$	1102*i*	251	1161*i*	172	849*i*	150
$f'^{high}_{model,i}$	1032*i*	75	836*i*	96	838*i*	95
$f'^{low}_{real,i}$	1013*i*	230	1089*i*	146	741*i*	124

[a]Due to rounding errors that become large as we take the differences of squares, these values are not consistent with the rounded values of the pseudofrequencies listed in this table. In the Supporting Information, we show the values with higher precision, which are consistent according to eq 16.

in the high level, the low level contributions to the frequency are 251 and 230 cm^{-1}, and the difference in the squares ($251^2 - 230^2 = 10101$) is much larger than the square of $f'^{high}_{model,i}$ ($75^2 = 5625$). This results in an imaginary ONIOM frequency. For the calculations with the 4-31G basis set in the high level, the differences in squares are smaller than the square of the high level contribution from the model system, resulting in real ONIOM frequencies.

The difference between $f'^{low}_{model,i}$ and $f'^{low}_{real,i}$ for the second mode is fairly similar for the calculations with STO-3G and 4-31G in the high level (21−26 cm^{-1}), but the absolute values are much higher with STO-3G than with 4-31G (which, of course, results in a much larger difference of the squares). This is surprising, since it is not the basis set of the low level method that is being changed, but the basis set of the high level method. The explanation is that the direction of the normal mode must be sufficiently affected by the change in basis set of the high level method for the curvature contributions from the low level

subcalculations to change so greatly, although the curvature contribution from the high level calculation on the model system does not change much. This strong dependence and different response from the high and low level calculations may indicate that at least one of the method combinations is not good and would need to be investigated further before production calculations are started.

Further exploration of the ONIOM(CAS(6,6)/STO-3G:HF/STO-3G) potential surface away from the C_s seam determined the location of an asymmetric transition structure. While the IRC from the symmetric second order saddle point along the mode that preserves C_s symmetry leads directly to the product, the IRC from the asymmetric TS leads to a different, diradical species. Thus, the spurious imaginary frequency may yield qualitatively different results when the potential surface is investigated. Although spurious imaginary frequencies may also occur for equilibrium structures, the consequences will only be small errors in the energies, as reaction paths will not be affected.

The bonds we cut in maleic anhydride to obtain the model system are formally single. However, the carbon atoms involved are sp^2 hybridized, and this bond will have some double bond character. To investigate to what extent this affects our findings, we performed additional calculations with the carbonyl groups substituted for two methyl groups, thus cutting a bond between sp^2 and sp^3 hybridized carbon atoms (in the symmetric TS, the carbon−carbon bond length stretches from 1.52 Å for the sp^2−sp^2 bond to 1.54 Å for the sp^2−sp^3 bond). The results are described in detail in the Supporting Information. At the target level of theory, there is a single imaginary frequency, but using ONIOM(CASSCF/STO-3G:HF/STO-3G), we again find an additional imaginary frequency. The only difference is that for CHD + maleic anhydride all the pseudofrequencies of the 'spurious mode' are real, while for the methylated system only two out of three pseudofrequencies are real. Thus, the introduction of spurious imaginary frequencies is not related to the sp^2 hybridized carbon atoms connecting the ONIOM layers

CONCLUSIONS

We developed a method to analyze ONIOM vibrational frequencies and their associated normal modes in terms of contributions from the individual subcalculations. This analysis does not increase the computational cost over a standard ONIOM frequency calculation.

We presented two case studies involving Diels−Alder cycloadditions: maleic anhydride and cyclohexadiene, and quinodimethane to a (5,5) SWNT. For certain ONIOM method combinations and partitions, both systems show a second imaginary vibrational frequency when the TS is optimized in C_s symmetry. For the cycloaddition reaction of quinodimethane and a (5,5) SWNT, the target PES also shows the second imaginary frequency; thus, the ONIOM extrapolation reproduces the target correctly at a significantly lower computational cost. In contrast, for the cycloaddition of maleic anhydride and cyclohexadiene, the target PES does not show the second imaginary frequency; thus, the ONIOM extrapolation does not reproduce the target correctly. Surprisingly, when we analyzed the individual ONIOM components of the second imaginary frequencies, we only found positive curvatures in both cases.

It is interesting to observe that, for one system studied here, three subcalculations all with positive curvatures correctly combine to give an imaginary frequency with ONIOM in C_s symmetry, while in the other case, three positive curvatures incorrectly give the same result. Furthermore, in the case of the correct second imaginary frequency (quinodimethane + (5,5) SWNT), the reaction path from the asymmetric first order TS on the ONIOM PES yields the same product as obtained with the target PES, while in the case of the incorrect imaginary frequency (maleic anhydride + cyclohexadiene), the reaction path from the asymmetric first order TS on the ONIOM PES yields a product different from that obtained with the target PES.

These two case studies demonstrate how the decomposition of ONIOM frequencies presented here highlights possible method incompatibility and incorrect description of the substituent effect, which may not be reflected in the corresponding reaction energetics. Although we cannot state that an imaginary frequency resulting from components with only positive curvatures is correct or incorrect, we can conclude that such modes should be treated with caution. In such cases, we suggest further exploratory work to ensure that ONIOM represents the target potential surface. One can improve the low level basis set or the level of theory until results no longer change (convergence is reached). Also, the calculations on the model system alone (truncated system) or on the full system at the low level of theory (truncated method) may be used to ensure that the ONIOM results are chemically sensible. An interesting observation in the current work is that the ONIOM energy difference between the symmetric TS and the asymmetric TS is much larger for maleic anhydride + cyclohexadiene (3.9 kcal·mol^{-1}) than for quinodimethane + (5,5) SWNT (0.2 kcal·mol^{-1}), which may indicate the extent to which the potential surface is affected and agrees with the target.

We hope that further studies for both ground and excited state processes will provide more insight into the behavior of the ONIOM frequency integration/Hessian deconstruction.

ASSOCIATED CONTENT

Supporting Information

Cartesian coordinates and energies of saddle points in the 5,5 SWNT + quinodimethane and cyclohexadiene + maleic anhydride systems calculated at target, (low, real) and ONIOM levels of theory. High precision (4 d.p.) pseudofrequencies for ONIOM saddle points. Further discussion, energies, coordinates and pseudofrequencies of symmetric structures in the cyclohexadiene + $C_2H_2(C(CH_3)_2)_2O$ system at target and ONIOM levels of theory. This information is available free charge via the Internet at http://pubs.acs.org/.

AUTHOR INFORMATION

Corresponding Author

*E-mail: m.bearpark@imperial.ac.uk.

Notes

The authors declare no competing financial interest.

ACKNOWLEDGMENTS

The U.K. Engineering and Physical Sciences Research Council (EPSRC) supported L.M.T. and S.M.L. via studentships. S.M.L. also acknowledges an Emerson Center Visiting Fellowship to work at Emory University with the group of Prof. Keiji Morokuma. We thank Dr. Mike Frisch (Gaussian, Inc.) for

helpful discussions. Calculations were run using the Imperial College High Performance Computing service.

REFERENCES

(1) Schlegel, H. B. *J. Comput. Chem.* **1982**, *3*, 214−218.
(2) Schlegel, H. B. *J. Comput. Chem.* **2003**, *24*, 1514−27.
(3) Warshel, A.; Levitt, M. *J. Mol. Biol.* **1976**, *103*, 227−249.
(4) Singh, U. C.; Kollman, P. A. *J. Comput. Chem.* **1986**, *7*, 718−730.
(5) Field, M. J.; Bash, P. A.; Karplus, M. *J. Comput. Chem.* **1990**, *11*, 700−733.
(6) Gao, J. In *Reviews in Computational Chemistry*; Lipkowitz, K. B.; Boyd, D. B., Eds.; VCH Publishers, Inc.: New York, 1996; pp 119−186.
(7) Riplinger, C.; Neese, F. *ChemPhysChem* **2011**, *12*, 3192−203.
(8) Kistler, K. A.; Matsika, S. *J. Phys. Chem. A* **2009**, *113*, 12396−403.
(9) Conti, I.; Altoè, P.; Stenta, M.; Garavelli, M.; Orlandi, G. *Phys. Chem. Chem. Phys.* **2010**, *12*, 5016−23.
(10) Svensson, M.; Humbel, S.; Froese, R. D. J.; Matsubara, T.; Sieber, S.; Morokuma, K. *J. Phys. Chem.* **1996**, *100*, 19357−19363.
(11) Vreven, T.; Morokuma, K. *J. Comput. Chem.* **2000**, *21*, 1419−1432.
(12) Hratchian, H. P.; Parandekar, P. V.; Raghavachari, K.; Frisch, M. J.; Vreven, T. *J. Chem. Phys.* **2008**, *128*, 034107.
(13) Montgomery, J. A., Jr.; Vreven, T.; Byun, K. S.; Komáromi, I.; Dapprich, S.; Morokuma, K.; Frisch, M. J. *J. Chem. Theory Comput.* **2006**, *2*, 815−826.
(14) Morokuma, K.; Musaev, D. G.; Vreven, T.; Basch, H.; Torrent, M.; Khoroshun, D. V. *IBM J. Res. Dev.* **2001**, *45*, 367−395.
(15) Bearpark, M. J.; Larkin, S. M.; Vreven, T. *J. Phys. Chem. A* **2008**, *112*, 7286−95.
(16) Dapprich, S.; Komáromi, I.; Byun, K. S.; Morokuma, K.; Frisch, M. J. *J. Mol. Struct.: THEOCHEM* **1999**, *461*, 1−21.
(17) Vreven, T.; Morokuma, K. *J. Phys. Chem. A* **2002**, *106*, 6167−6170.
(18) Frisch, M. J.; Trucks, G. W.; Schlegel, H. B.; Scuseria, G. E.; Robb, M. A.; Cheeseman, J. R.; Scalmani, G.; Barone, V.; Mennucci, B.; Petersson, G. A.; Nakatsuji, H.; Caricato, M.; Li, X.; Hratchian, H. P.; Izmaylov, A. F.; Bloino, J.; Zheng, G.; Sonnenberg, J. L.; Liang, W.; Hada, M.; Ehara, M.; Toyota, K.; Fukuda, R.; Hasegawa, J.; Ishida, M.; Nakajima, T.; Honda, Y.; Kitao, O.; Nakai, H.; Vreven, T.; Montgomery, Jr., J. A.; Peralta, J. E.; Ogliaro, F.; Bearpark, M.; Heyd, J. J.; Brothers, E.; Kudin, K. N.; Staroverov, V.; Keith, T.; N.; Kobayashi, R.; Normand, J.; Raghavachari, K.; Rendell, A.; Burant, J. C.; Iyengar, S. S.; Tomasi, J.; Cossi, M.; Rega, N.; Millam, J. M.; Klene, M.; Knox, J. E.; Cross, J. B.; Bakken, V.; Adamo, C.; Jaramillo, J.; Gomperts, R.; Stratmann, R. E.; Yazyev, O.; Austin, A. J.; Cammi, R.; Pomelli, C.; Ochterski, J. W.; Martin, R. L.; Morokuma, K.; Zakrzewski, V. G.; Voth, G. A.; Salvador, P.; Dannenberg, J. J.; Dapprich, S.; Pandekar, P. V.; Mayhall, N. J.; Daniels, A. D.; Farkas, Ö.; Foresman, J. B.; Ortiz, J. V.; Cioslowski, J.; Fox, D. J. *Gaussian Development Version, Revision H.13*; Gaussian, Inc.: Wallingford, CT, 2010.
(19) Hall, K. F.; Vreven, T.; Frisch, M. J.; Bearpark, M. J. *J. Mol. Biol.* **2008**, *383*, 106−21.
(20) Vreven, T.; Morokuma, K.; Farkas, O.; Schlegel, H. B.; Frisch, M. J. *J. Comput. Chem.* **2003**, *24*, 760−9.
(21) Vreven, T.; Frisch, M. J.; Kudin, K. N.; Schlegel, H. B.; Morokuma, K. *Mol. Phys.* **2006**, *104*, 701−714.
(22) Larkin, S. M.; Vreven, T.; Bearpark, M. J.; Morokuma, K. *Can. J. Chem.* **2009**, *87*, 872−879.
(23) Ando, K.; Morokuma, K. *Theor. Chem. Acc.* **2011**, *130*, 323−331.
(24) Lu, X.; Tian, F.; Wang, N. Q.; Zhang, Q. N. *Org. Lett.* **2002**, *4*, 4313−5.
(25) Clemente, F. R.; Vreven, T.; Frisch, M. J. In *Quantum Biochemistry*; Matta, C. F., Ed.; Wiley-VCH: Weinheim, 2010; pp 61−83.
(26) Osuna, S.; Morera, J.; Cases, M.; Morokuma, K.; Solà, M. *J. Phys. Chem. A* **2009**, *113*, 9721−6.
(27) Hratchian, H. P.; Schlegel, H. B. *J. Chem. Phys.* **2004**, *120*, 9918−24.
(28) Hratchian, H. P.; Schlegel, H. B. *J. Chem. Theory Comput.* **2005**, *1*, 61−69.
(29) Hayashi, T.; Kim, Y. A.; Natsuki, T.; Endo, M. *ChemPhysChem* **2007**, *8*, 999−1004.
(30) Bandaru, P. R. *J. Nanosci. Nanotechnol.* **2007**, *7*, 1239−1267.
(31) Zhao, Y.-L.; Stoddart, J. F. *Acc. Chem. Res.* **2009**, *42*, 1161−71.
(32) Kumar, I.; Rana, S.; Cho, J. W. *Chem.—Eur. J.* **2011**, *17*, 11092−101.
(33) Hirsch, A. *Angew Chem., Int. Ed.* **2002**, *41*, 1853.
(34) Filippone, S.; Barroso, M. I.; Martín-Domenech, A.; Osuna, S.; Solà, M.; Martín, N. *Chem.—Eur. J.* **2008**, *14*, 5198−206.
(35) Delgado, J. L.; Osuna, S.; Bouit, P.-A.; Martínez-Alvarez, R.; Espíldora, E.; Solà, M.; Martín, N. *J. Org. Chem.* **2009**, *74*, 8174−8180.
(36) Izquierdo, M.; Osuna, S.; Filippone, S.; Martín-Domenech, A.; Solà, M.; Martín, N. *J. Org. Chem.* **2009**, *74*, 6253−9.
(37) Izquierdo, M.; Osuna, S.; Filippone, S.; Martín-Domenech, A.; Solà, M.; Martín, N. *E. J. Org. Chem.* **2009**, 6231−6238.
(38) Osuna, S.; Houk, K. N. *Chem.—Eur. J.* **2009**, *15*, 13219−13231.
(39) Osuna, S.; Swart, M.; Solà, M. *J. Phys. Chem. A* **2011**, *115*, 3491−3496.
(40) Lu, X.; Tian, F.; Xu, X.; Wang, N. Q.; Zhang, Q. N. *J. Am. Chem. Soc.* **2003**, *125*, 10459−64.
(41) Lu, X.; Yuan, Q.; Zhang, Q. N. *Org. Lett.* **2003**, *5*, 3527−3530.
(42) Montoya, A.; Mondragón, F.; Truong, T. N. *Carbon* **2002**, *40*, 1863−1872.
(43) Wang, H.; Xu, J. *Chem. Phys. Lett.* **2009**, *477*, 176−178.
(44) Chu, Y.-Y.; Su, M.-D. *Chem. Phys. Lett.* **2004**, *394*, 231−237.
(45) Wanno, B.; Du, A. J.; Ruangpornvisuti, V.; Smith, S. C. *Chem. Phys. Lett.* **2007**, *436*, 218−223.
(46) Basiuk, V. A. *J. Phys. Chem. B* **2003**, *107*, 8890−8897.
(47) Basiuk, V. A. *J. Comput. Theor. Nanosci.* **2004**, *1*, 7.
(48) Basiuk, V. A. *J. Nanosci. Nanotechnol.* **2004**, *4*, 1095−1101.
(49) Liu, L. V.; Tian, W. Q.; Wang, Y. A. *J. Phys. Chem. B* **2006**, *110*, 1999−2005.
(50) Castillo, Á.; Lee, L.; Greer, A. *J. Phys. Org. Chem.* **2012**, *25*, 42−49.
(51) Trzaskowski, B.; Adamowicz, L. *Theor. Chem. Acc.* **2009**, *124*, 95−103.
(52) Wang, L.; Yi, C.; Zou, H.; Gan, H.; Xu, J.; Xu, W. *J. Mol. Model.* **2011**, *17*, 2751−2758.
(53) Cao, Y.; Houk, K. N. *J. Mater. Chem.* **2011**, *21*, 1503.
(54) Yuan, Y.; Chen, P.; Ren, X.; Wang, H. *ChemPhysChem* **2012**, *13*, 741−50.
(55) Hine, N. D. M.; Robinson, M.; Haynes, P. D.; Skylaris, C. K.; Payne, M. C.; Mostofi, A. A. *Phys. Rev. B* **2011**, *83*, 195102.
(56) Bearpark, M. J.; Ogliaro, F.; Vreven, T.; Boggio-Pasqua, M.; Frisch, M. J.; Larkin, S. M.; Morrison, M.; Robb, M. A. *J. Photochem. Photobiol., A* **2007**, *190*, 207−227.